ADVANCED HEALTHCARE MATERIALS
www.advhealthmat.de

Polymersomal Poly(I:C) Self-Magnifies Antitumor Immunity by Inducing Immunogenic Cell Death and Systemic Immune Activation

Jingyi Wang, Beibei Guo, Zhiwei Sun, Songsong Zhao, Li Cao, Zhiyuan Zhong, and Fenghua Meng**

Immunotherapy has emerged as a powerful weapon against lung cancer, yet only a fraction of patients respond to the treatment. Poly(I:C) (PIC) effectively triggers both innate and adaptive immunity. It can also induce immunogenic cell death (ICD) in tumor cells. However, its efficacy is hindered by its instability in vivo and limited cellular uptake. To address this, PIC is encapsulated in cRGD-functionalized polymersomes (t-PPIC), which significantly increases its stability and uptake, thus activating dendritic cells (DCs) and inducing apoptosis of lung tumor cells in vitro. In a murine LLC lung tumor model, systemic administration of t-PPIC effectively suppresses tumor growth and leads to survival benefits, with 40% of the mice becoming tumor-free. Notably, t-PPIC provokes stronger apoptosis and ICD in tumor tissue and elicits a more potent stimulation of DCs, recruitment of natural killer (NK) cells, and activation of $CD8^+$ T cells, compared to free PIC and nontargeted PPIC controls. Furthermore, when combined with immune checkpoint inhibitors or radiotherapy, t-PPIC amplifies the antitumor immune response, resulting in complete regression in 60% of the mice. These compelling findings underscore the potential of integrin-targeted polymersomal PIC to enhance antitumor immunity by simultaneously inducing ICD and systemic immune activation.

1. Introduction

Immunotherapy appears to be a powerful strategy for treating different malignancies, including melanoma and lung cancers.[1] Unfortunately, even for lung cancer patients who are most commonly treated with immunotherapy, only a small portion is eligible and responds to treatment. Current immune checkpoint blockade (ICB) therapy based on programmed death 1/programmed death ligand 1 (PD-1/PD-L1) and cytotoxic T lymphocyte-associated antigen-4 (CTLA-4) was effective for only ≈25% of non-small cell lung cancer (NSCLC) patients.[2] To improve the response rate to immunotherapy, ongoing research has focused on sensitizing tumor cells to ICB,[1a] increasing the immunogenicity of tumor cells, employing potent immunoadjuvants, and reducing the immunosuppressive tumor microenvironment.[3] Toll-like receptor-3 (TLR3) is primarily expressed on the endosomes of antigen-presenting cells (APCs). It detects viruses and host-derived nucleic acids, triggers inflammatory pathways, and activates the innate immune response. Poly(I:C) (PIC), a synthetic dsRNA and potent TLR3 agonist, can bind to TLR3 and activate APCs, leading to the stimulation of both innate and adaptive immunity[4] and the production of cytokines such as type-I interferon (IFN-I).[5] IFN-I can recruit and activate dendritic cells (DCs) and natural killer (NK) cells, and enhance antigen-specific $CD8^+$ T-cell responses. Therefore, PIC can regulate the immune microenvironment in tumors. Notably, TLR3 has also been found to be expressed in various cancer cells, including lung, breast, prostate, and liver cancer cells.[6] Studies have shown that the binding of PIC to TLR3 can induce the apoptosis and immunogenic cell death (ICD) of cancer cells by upregulating antitumor genes,[7] leading to the release of damage-related molecular patterns (DAMPs) to act as tumor antigens.[8] These in situ-generated tumor antigens can promote APC maturation and activate tumor-specific cytotoxic T lymphocytes (CTLs), contributing to an antitumor immune response.[9]

The polyribonucleotide nature of PIC makes it vulnerable in vivo and has poor cellular uptake,[4] posing a great challenge for antitumor application. To overcome this, various types of

J. Wang, B. Guo, Z. Sun, S. Zhao, Z. Zhong, F. Meng
Biomedical Polymers Laboratory
College of Chemistry
Chemical Engineering and Materials Science
and State Key Laboratory of Radiation Medicine and Protection
Soochow University
Suzhou 215006, P. R. China
E-mail: zyzhong@suda.edu.cn; fhmeng@suda.edu.cn
L. Cao, Z. Zhong
College of Pharmaceutical Sciences
Soochow University
Suzhou 215006, P. R. China
Z. Zhong
International College of Pharmaceutical Innovation
Soochow University
Suzhou 215006, P. R. China

The ORCID identification number(s) for the author(s) of this article can be found under https://doi.org/10.1002/adhm.202400784

DOI: 10.1002/adhm.202400784

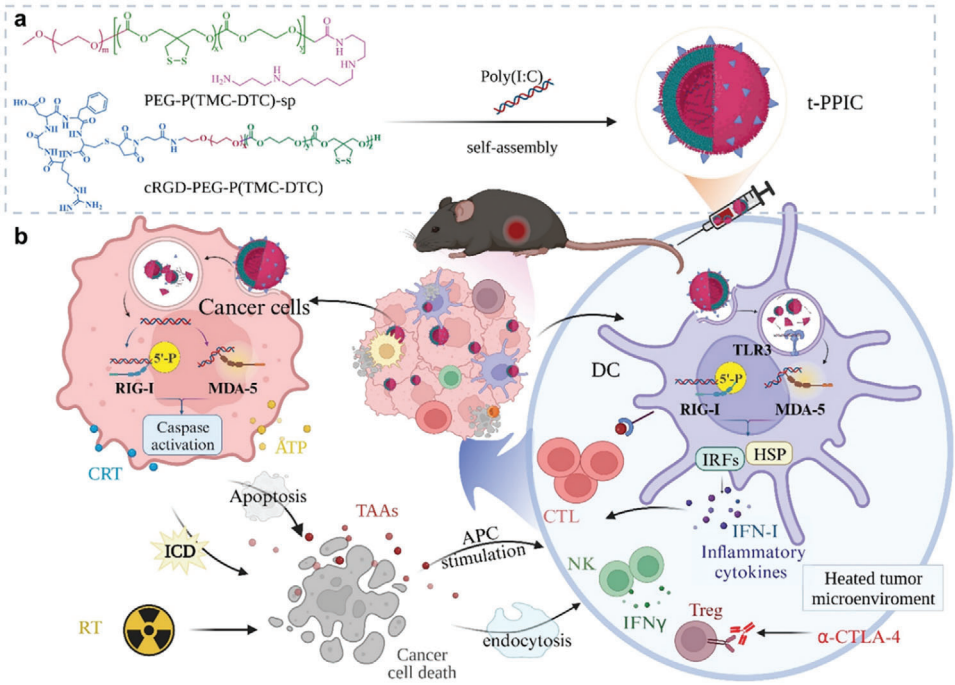

Scheme 1. Schematic illustration of integrin-targeted nanodelivery of poly(I:C) (t-PPIC): a) preparation and b) antitumor mechanism of immunotherapy in murine LLC lung cancer.

nanoparticles (NPs) such as polymeric NPs, lipid NPs, gold NPs, mineral salts, and membrane-coated NPs have been used to carry PIC to enhance its stability and cellular uptake through electrostatic interactions.[10] For example, Liu et al. reported that poly(lactic-*co*-glycolic acid) (PLGA) NPs coloaded with PIC and tumor lysate elicited strong tumor-specific immune responses in mouse models.[11] While many PIC-loaded NPs are larger than 100 nm, studies suggest that smaller NPs, especially those smaller than 100 nm, are more efficiently taken up by APCs.[12] Additionally, NPs with a size of ≈50 nm demonstrate highly effective uptake and retention within lymph nodes.[13] However, challenges such as large size, uncontrolled drug enrichment, complex preparation, and poor biocompatibility hinder the further development of these materials. In contrast, polymersomes offer clear advantages,[14] including controlled and efficient loading of nucleic acids, small and uniform sizes, easy preparation, good biocompatibility, a clear tumor-targeting mechanism, and the ability to coload different drugs for effective combination tumor therapy.[15]

Here, we report for the first time that cyclic RGD peptide (cRGD)-modified disulfide-crosslinked polymersomes mediate high-efficacy targeted intracellular delivery of PIC to both lung tumor cells and APCs that overexpress $\alpha_v\beta_3$ and $\alpha_v\beta_5$ integrins (**Scheme 1**). These integrins are highly elevated in malignant cells and tumor neovasculatures compared to normal cells. cRGD has demonstrated targetability to these integrins,[16] and a cRGD-based conjugate, cRGD-ZW800-1, has advanced to phase II clinical trials for intraoperative NIR imaging in patients.[17] These targeted polymersomal poly(I:C) (t-PPIC) have many merits: (i) as previously reported for siRNA transfection,[18] it is highly effective and particularly stable; (ii) it can boost the proliferation and maturation of DCs by efficiently releasing PIC to APCs; (iii) it can induce strong ICD by directing PIC to lung cancer cells; and (iv) it may serve as an in situ vaccine to promote a positive antitumor response in a mouse model. Strikingly, our results showed that systemic administration of t-PPIC induced significant antitumor immunity, resulting in complete regression in 40% of LLC lung tumor-bearing mice. Therefore, integrin-targeted polymersomal poly(I:C) offers potent self-enhanced and systemic immunotherapy for solid tumors.

2. Results and Discussion

2.1. Fabrication and Characterization of the Nano-TLR3 Agonist (t-PPIC)

The PIC utilized in this study is a synthetic double-stranded RNA that has been frequently used as an immunoadjuvant in animal studies[10b] and human clinical trials.[19] The negative charge and vulnerability of the PIC greatly limit its activity in vivo. In this study, integrin-targeting poly(I:C)-loaded polymersomes (t-PPIC) and a nontargeted control (PPIC) were created by self-assembly of PEG-P(TMC-DTC)-spermine with and without cRGD-PEG-P(TMC-DTC) (15 mol.%), respectively, in PIC-containing buffers. Both the obtained t-PPIC and PPIC had high drug-loading efficacy and loading content (DLC up to 19 wt.%), a uniform size ≈52 nm) and high reproducibility (**Figure 1a**; Table S1, Supporting Information). TEM images of PPIC and t-PPIC revealed a typical hollow vesicular structure with average sizes of 45.8 ± 7.5 nm and 49.2 ± 6.0 nm, respectively, in the dry state (Figure 1b). The polymersomes achieved high PIC loading efficiencies despite the high molecular weight and distribution of PIC (200–1000 bp).

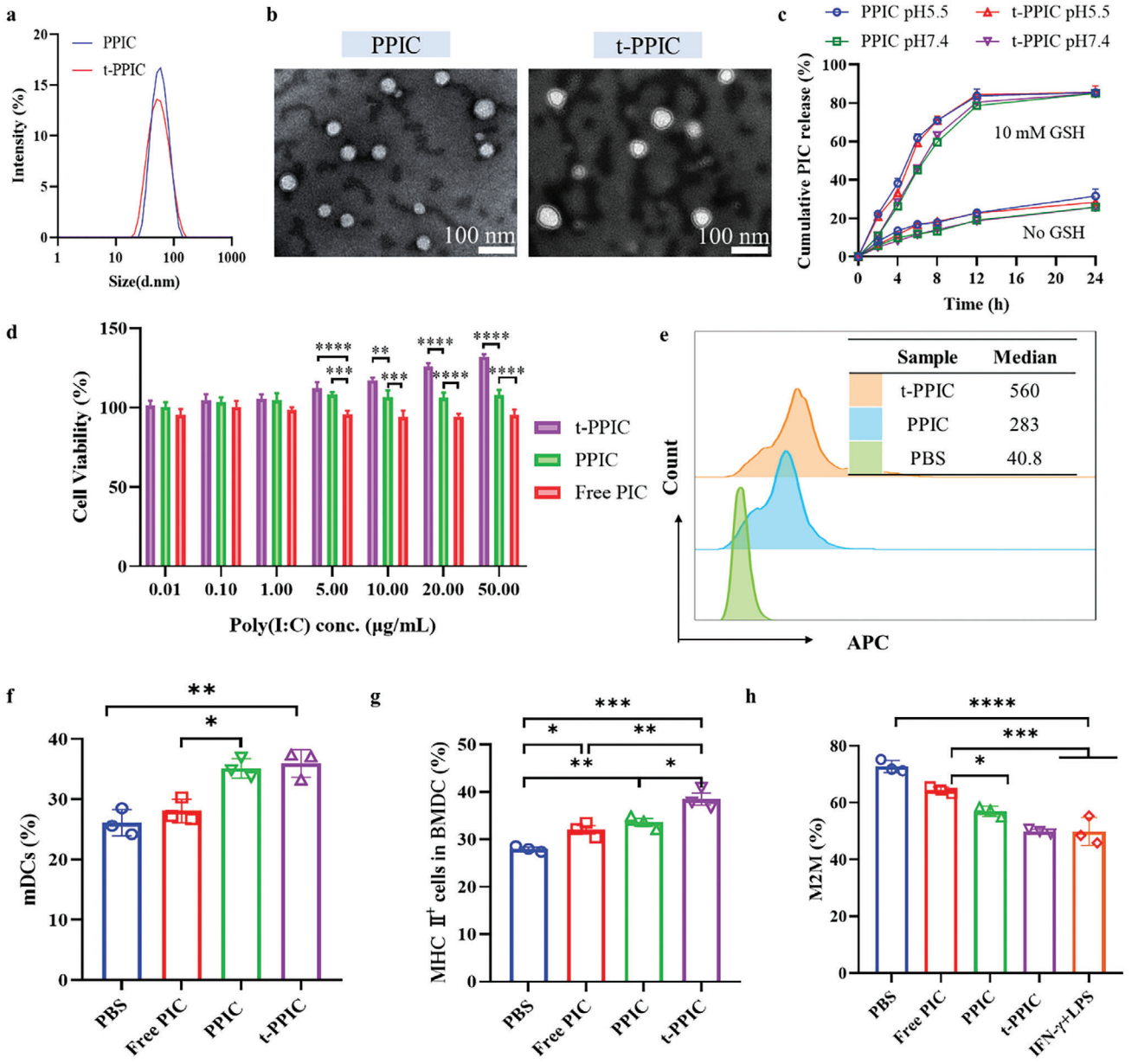

Figure 1. Physicochemical properties of t-PPIC and PPIC and their effects on immune cells. a) Size and distribution determined using DLS, b) TEM micrographs, and c) PIC release profiles of t-PPIC and PPIC under various conditions. d) Viability (24 h incubation, n = 6) and e) uptake (4 h incubation) of BMDCs treated with t-PPIC or PPIC. Percentages of f) mDCs and g) MHC II$^+$ mDCs, and h) percentages of the M2 phenotype in BMDMs treated with t-PPIC or PPIC (n = 3). *$p < 0.05$, **$p < 0.01$, ***$p < 0.001$ and ****$p < 0.0001$.

This was mainly attributed to the strong electrostatic interactions and hydrogen bonding between the dense negative charge of PIC and the positive charge of the spermine inner shell of the polymersomes. Additionally, the disulfide-crosslinked polymersome membrane, which spontaneously formed during the self-assembly process, provided a barrier preventing drug leakage. These polymersomes have demonstrated a high loading capacity for cyclic dinucleotides and proteins.[15a,20] Moreover, both PPIC and t-PPIC showed good stability during storage and in 10% FBS, as well as reduction-responsive destabilization triggered by 10 mM GSH (Figure S1a–c, Supporting Information), as observed in other DTC nanostructures.[15f] Gel electrophoresis images confirmed the high and stable loading of PIC inside the polymersomes and the GSH-triggered PIC release at pH 7.4 and pH 5.5, respectively (Figure S1d, Supporting Information). In accordance with these results, the in vitro drug release profiles demonstrated that the release of PIC, a large molecular drug, from the polymersomes was slow under blood-mimicking conditions (PB, pH 7.4) but strongly increased under cytosol-mimicking reductive conditions (PB, pH 7.4, 10 mM GSH) and endosomal conditions (PB, pH 5.5, 10 mM GSH), facilitating the binding of PIC to RIG-I and MDA-5 in the cytosol or to TLR3 in the inner membrane of the endosome, respectively (Figure 1c). These results confirm that t-PPIC can be easily prepared with small sizes,

stable and efficient PIC loading, and reduction-triggered drug release.

2.2. Effect of t-PPIC and PPIC on Primary Immune Cells

Stimulation of the TLR3 pathway to induce IFN-α/β production is the most important action of PIC as an immunostimulant. To investigate the effect of the nano-TLR3 agonist on immune cells, we measured TLR3 expression in primary immune cells, Bone Marrow-Derived Dendritic Cells (BMDCs), Bone Marrow-Derived Macrophages (BMDMs) and their stimulated phenotypes. Flow cytometric analysis revealed that the membranes of both immature and mature BMDCs exhibited ≈1.8-fold greater TLR3 expression than did the membranes of untreated cells. While the total TLR3 expression increased 4.8- and 4.2-fold, respectively (Figure S2a,b, Supporting Information), confirming high intracellular TLR3 expression. BMDMs and M1 macrophages displayed similar trends but had lower TLR3 levels in both the membrane and total amount (Figure S2c,d, Supporting Information). The influence of PPIC and t-PPIC on the viability, uptake, and activation of immune cells was also studied. The CCK8 assay results showed that free PIC and PPIC after 24 h of incubation were not toxic to BMDCs, in agreement with the reported nontoxicity of PIC to immune cells.[21] Whereas t-PPIC promoted cell proliferation at PIC concentrations above 5 μg mL^{-1} (***p, Figure 1d). The endocytosis of Cy5-labeled t-PPIC in BMDCs after 4 h of incubation was twofold greater than that of PPIC (Figure 1e), in accordance with the upregulation of $\alpha_v\beta_3$ in BMDCs.[22] Nonetheless, t-PPIC and PPIC promoted a similar degree of BMDC maturation, ≈10% greater than that in the PBS and free PIC groups (**p, Figure 1f). The DC stimulation effect was much less than that of CpG or immune checkpoint inhibitors,[23] although free PIC was reported to induce DC activation in tumor-draining lymph nodes (TdLNs) in vivo[24] and has been applied in clinical trials.[25] This discrepancy might be attributable to the fact that PIC mainly stimulates conventional DCs (cDC1) in vivo[26] to release IFN-I and activate NK cells, which can ultimately promote T-cell activation in the tumor microenvironment. Moreover, when coincubated with model antigen (ovalbumin, OVA), t-PPIC-treated BMDCs exhibited significantly greater MHC II$^+$ antigen presentation than did those in the PBS (***p), free PIC (**p) and PPIC (*p) groups (Figure 1g), confirming their capacity to present specific antigens. Furthermore, compared with free PIC and PBS, t-PPIC transformed significantly more M2 macrophages into M1 macrophages (***p), to a level similar to that of cells stimulated with LPS and IFN-γ (Figure 1h). M2 macrophages are major immunosuppressive tumor-associated macrophages (TAMs). A decrease in TAMs may further drastically increase the secretion of TNF-α and IL-6 and activate immune cells such as NK cells, DCs, and CTLs.[5]

2.3. Effect of t-PPIC and PPIC on Tumor Cells

Consistent with the high expression of $\alpha_v\beta_3$ and $\alpha_v\beta_5$ in LLC cells,[27] t-PPIC clearly promoted endocytosis more than did PPIC. (**Figure 2a**). The CCK-8 assay results demonstrated that both PPIC and t-PPIC caused moderate cell death (> 75% cell viability), even at high concentrations and after 48 h of incubation (Figure 2b). Surprisingly, compared with free PIC and PBS, PPIC and t-PPIC greatly inhibited colony formation in LLC cells, with hardly any colonies in the t-PPIC group at 50 μg mL^{-1} (Figure 2c). Interestingly, LLC cells experienced overwhelming increases in early and late apoptosis after incubation with t-PPIC (72.4%, ****p) or PPIC (36.2%) at a low concentration (10 μg mL^{-1}) (Figure 2d), in sharp contrast to free PIC, which did not induce significant apoptosis. It was reported that free PIC at 100 μg mL^{-1} induced the apoptosis of H460 cells via caspase-8 activation.[7] The improved apoptotic activity of t-PPIC and PPIC is likely due to their enhanced cellular uptake. Apoptosis can occur via intrinsic (i.e., caspase-9 and bcl-2 apoptosis-related proteins) or extrinsic (Fas-associated protein death domain-caspase-8 pathway) pathways in tumor cells.[6a,7] Flow cytometry showed that LLC cells had 1.67- to 2.11-fold greater TLR3 expression intracellularly than on the surface (using MC38, GL261, and fibroblast L929 cells as controls) (Figure S2e–h, Supporting Information), in accordance with reports on TLR3 expression in certain tumor cells.[7,28] Therefore, intracellularly delivered PIC may be responsible for apoptosis via the TLR3, Ifih1, or Ddx58 pathway.

Previously, we reported that apoptotic cells induced by granzyme B or LTX 315 peptide were immunogenic.[20,29] To investigate whether t-PPIC could induce ICD in LLC cells, ATP release and surface exposure of CRT, typical ICD markers, were measured. The results showed that the two markers displayed the same trend as apoptosis: t-PPIC > PPIC > free PIC > PBS. In particular, 10 μg mL^{-1} t-PPIC induced significantly more ICD than 10 μg mL^{-1} PPIC (***p) (Figure 2e,f). These results confirm that apoptotic LLC cells induced by t-PPIC are highly immunogenic and can release "eat-me" signals and apoptotic bodies that contain tumor antigens for immune stimulation.[6a,7,28] In addition, t-PPIC treatment also caused ICD in 4T1 and GL261 tumor cells, and the levels of both CRT and ATP were significantly greater than those in the PPIC group (Figure S3, Supporting Information), which was probably due to the expression of TLR3, RIG-I, and MDA-5 in these two cell lines. Nonetheless, ATP secretion in these cells was much lower than in LLC cells. Further investigation of the effect of ICD on LLC cells induced by t-PPIC and PPIC on BMDC stimulation revealed that the percentage of mature DCs (mDCs) activated by t-PPIC/LLC cells was significantly greater than that activated by PPIC/LLC cells (**p) or PBS (****p) (Figure 2g). Overall, fewer mDCs were observed compared to those without tumor cells, possibly due to the consumption of PIC formulations by LLC cells before they entered BMDCs. Taken together, it is evident that t-PPIC can actively target LLC cells and DCs via an integrin-mediated mechanism.

2.4. RNA-Seq Analysis of DCs and LLC Cells Treated with PIC Formulations

To investigate the pathway by which PIC formulations may influence DCs and LLC cells, RNA-seq was performed to explore the gene expression of TLR3, Ifih1 (MDA-5), and Ddx58 (RIG-I), which are important for PIC function.[10b,30] Heatmap analysis revealed ≈60-, 80-, and 5-fold greater expression of TLR3, Ifih1, and Ddx58, respectively, in DCs than in LLC cells (Figure

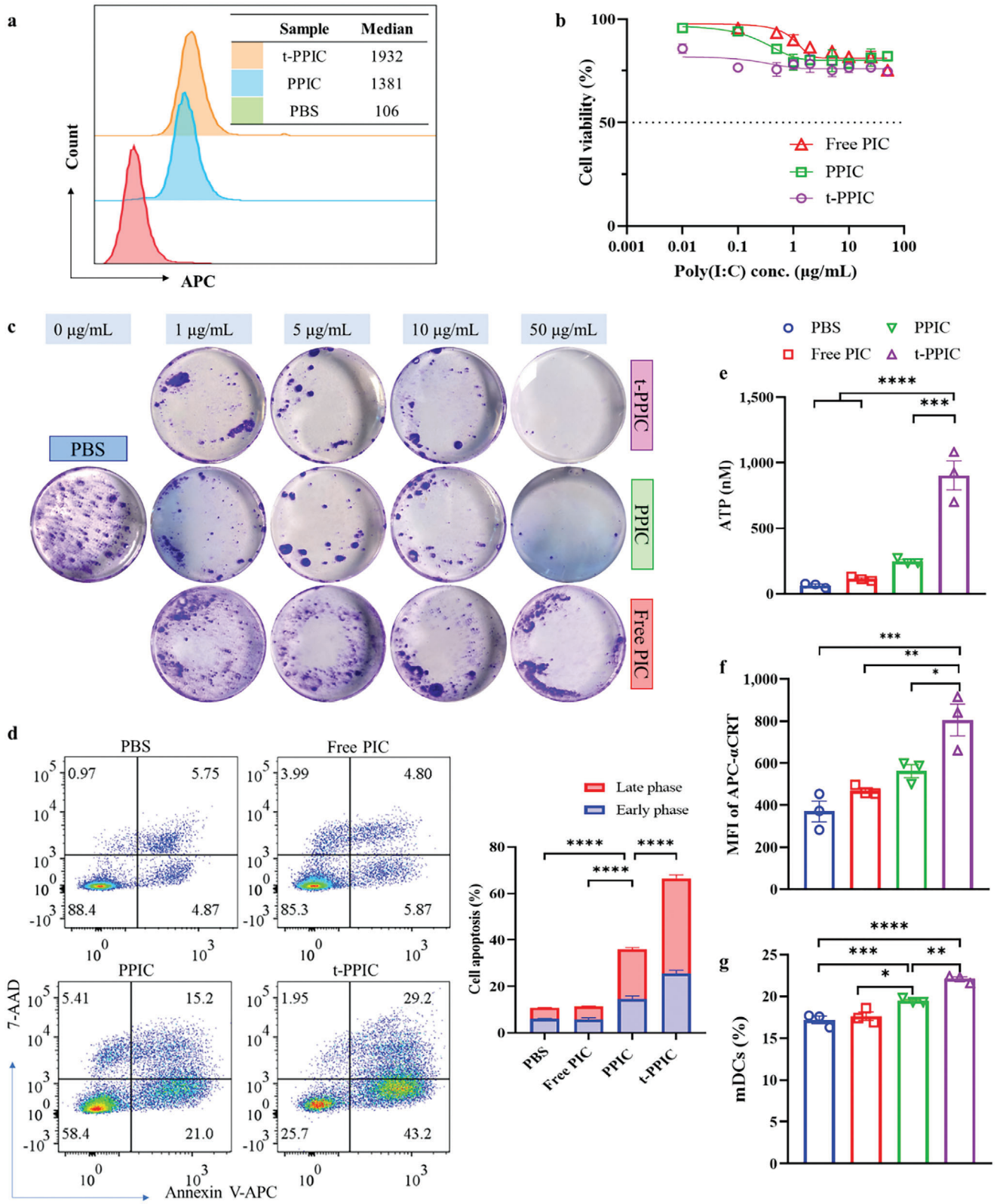

Figure 2. Effect of t-PPIC and PPIC on tumor cells. a) Endocytosis and b) cell viability (n = 6) of LLC cells treated with t-PPIC or PPIC. c) Colony formation and d) apoptosis (n = 4) after 48 h of incubation. Induction of e) ATP and f) CRT after 24 h of incubation (n = 3). g) Content of mDCs after 24 h of costimulation with LLC cells and t-PPIC (n = 3). For d)-g), the PIC concentration was 10 μg mL^{-1}. *$p < 0.05$, **$p < 0.01$, ***$p < 0.001$ and ****$p < 0.0001$.

S2i, Supporting Information). Treatment with free PIC and t-PPIC appeared to affect LLC cells and DCs via different pathways. In LLC cells, free PIC functioned mainly via TLR3, and t-PPIC functioned mainly via the Ifih1 and Ddx58 pathways (**Figure** 3a). In DCs, three pathways were important for both treatments (Figure 3b).

The RNA-seq heatmaps of LLC cells and DCs showed that treatments with PIC formulations induced vastly different gene expression patterns, including changes in apoptosis, migration, and defense system genes. For LLC cells, the apoptosis induced by t-PPIC most likely occurred via the extrinsic pathway, which highly upregulated casp1, casp2, casp4, casp6, casp7, casp8, and casp12, while intrinsic pathway markers (e.g., casp3/9) were downregulated or unchanged (Figure 3a). In t-PPIC-treated LLC cells, the expression of the HMGB1 and ATP genes (ICD markers), Mapk gene (Mapk/Erk pathway), and Pidd1 gene (P53 onco-suppressive protein) was highly promoted, while the expression of the Cdk genes (cell cycle, colony formation), Thbs1 gene, and ApoE gene (migration) was downregulated compared to that in the free PIC group (Figure 3a). According to the volcano plots, t-PPIC increased the expression of 173 genes and decreased the expression of 533 genes in LLC cells compared to those in the PBS group. Compared to those in the free PIC group, t-PPIC increased the expression of 202 genes and decreased the expression of 362 genes (Figure S4a–c, Supporting Information). GO analysis revealed that in contrast to no influence of free PIC, t-PPIC strongly promoted the innate immune response, such as responses to wounding, organisms, and protozoans (Figure 3c). The stimulation of nonimmune cells with defense functions has rarely been reported. In addition, the circadian sleep/wake cycle seemed to be altered in the t-PPIC group compared with the free PIC group, indicating that t-PPIC regulates the proliferation, DNA repair, apoptosis, metabolism, and stemness of LLC cells.[31]

The heatmaps of DCs treated with t-PPIC revealed strong increases in the expression of innate immunity-related genes (e.g., IFN and Nfkb) and chemokine ligand genes (e.g., Cxcl1: activation of nuclear factor-κB; Cxcl10: recruitment of T cells and NK cells; Ccl3/5: recruitment of monocytes and macrophages), the downregulation of some chemokine receptor genes (e.g., Cxcr4: migration and proliferation of stem cells and progenitor cells) and the expression of apoptosis-related genes (Figure 3b). Volcano plots illustrated that significantly more genes were altered in DCs than in LLC cells by PIC formulations. The t-PPIC induced upregulation of 3896 genes/downregulation of 3678 genes and upregulation of 994 genes/downregulation of 969 genes compared to those in the PBS and free PIC groups, respectively (Figure 3d; Figure S4e, Supporting Information). Both t-PPIC and free PIC strongly upregulated the hspa1 gene (innate immune-related gene) and downregulated the CD163, Fn1, and Tifab genes (inflammation-related genes) (Figure S4d,e, Supporting Information). The t-PPIC further induced the expression of more innate immune-related genes, such as cck, cxcl3, mt3, and rn7sk, and less inflammation-related genes, such as epx, c3, adgre4, and prg2, than what free PIC did (Figure 3d). GO analysis revealed that t-PPIC and free PIC were highly differentially expressed genes involved in the regulation of defense response, cell response to IFN-β, leukocyte chemotaxis, and migration (Figure S5a,b, Supporting Information). Compared with free PIC, t-PPIC prompted the inflammatory response, positive regulation of cell activation, leukocyte migration, zymogen activation, and cellular extravasation (Figure 3e). In addition, t-PPIC drastically altered genes on the external side of the plasma membrane and carbohydrate binding compared to those in the free PIC group. t-PPIC caused differences in genes related to the extracellular matrix and G-protein coupled receptor activity compared to those in the PPIC group (Figure S5c, Supporting Information), in line with the interaction of cRGD with the DC membrane (Figure S2, Supporting Information).

It is evident that t-PPIC more effectively inhibits the proliferation and colony formation, and promotes apoptosis and ICD of LLC cells than does PPIC, which can further more strongly activate APCs. The colocalization of TLR agonists with tumor antigens might lead to a minimal in situ tumor vaccine that enables a potent antitumor immune response.

2.5. Therapeutic Activity of t-PPIC and PPIC in a Subcutaneous LLC Mouse Model

The antitumor activity of t-PPIC was evaluated in a subcutaneous LLC tumor model (**Figure** 4a). The impact of dosage and administration route was investigated. The results showed that all t-PPIC treatments, whether administered via intravenous (i.v.) or intratumoral (i.t.) injection, effectively slowed down tumor growth (Figure 4b). The i.v. injection of t-PPIC at 3.75 mpk had a similar inhibitory effect to the i.t. injection at 1.25 mpk. The i.v. administration of t-PPIC at various doses ranging from 3.75 to 7.5 mpk showed an optimal therapeutic effect at 5 mpk, resulting in two out of five mice becoming tumor-free, as indicated in the spider plots (Figure 4c). As expected, t-PPIC outperformed PPIC at the same dosage of 5 mpk. Notably, none of the treatments caused substantial body weight loss (Figure 4d), indicating the safety of t-PPIC. Additionally, mice treated with t-PPIC at 3.75, 5.0, and 7.5 mpk (i.v.) had median survival times (MSTs) of 30, 45, and 36 days (versus 18 days for PBS, **p), respectively (Figure 4e). t-PPIC at 3.75 mpk i.v. and 1.25 mpk i.t. both led to 20% tumor-free mice. In contrast, free PIC administered i.v. or i.t. administration was found to be ineffective for treating LLC tumors.[32] The high antitumor activity of t-PPIC is attributed to its better retention effect due to its small size, increased binding to tumor neovasculature, and/or enhanced uptake by LLC cells and APCs (Figures 1e and 2a) compared to free PIC. We have shown previously that polymersomal CDNs injected intratumorally are distributed to the blood circulation at a much slower rate than free CDNs.[33] Unlike free PIC, which is primarily administered through local injection for antitumor purposes,[21] t-PPIC can also be injected via i.v. injection, seemingly inducing a stronger systemic immune response, as reported by Seder.[34]

A biodistribution study of Cy5-labeled t-PPIC and PPIC in LLC mice showed that t-PPIC accumulated much more in the tumors than did PPIC at 6 h and further increased at 24 h (Figure S6, Supporting Information), which was attributable to the binding of cRGD to $\alpha_v\beta_3$ and $\alpha_v\beta_5$ integrins on LLC cells and tumor neovasculatures. Moreover, t-PPIC, especially at 24 h, was highly deposited in immune organs, such as the spleen and lymph nodes, which may enable systemic and potent stimulation of immune cells.

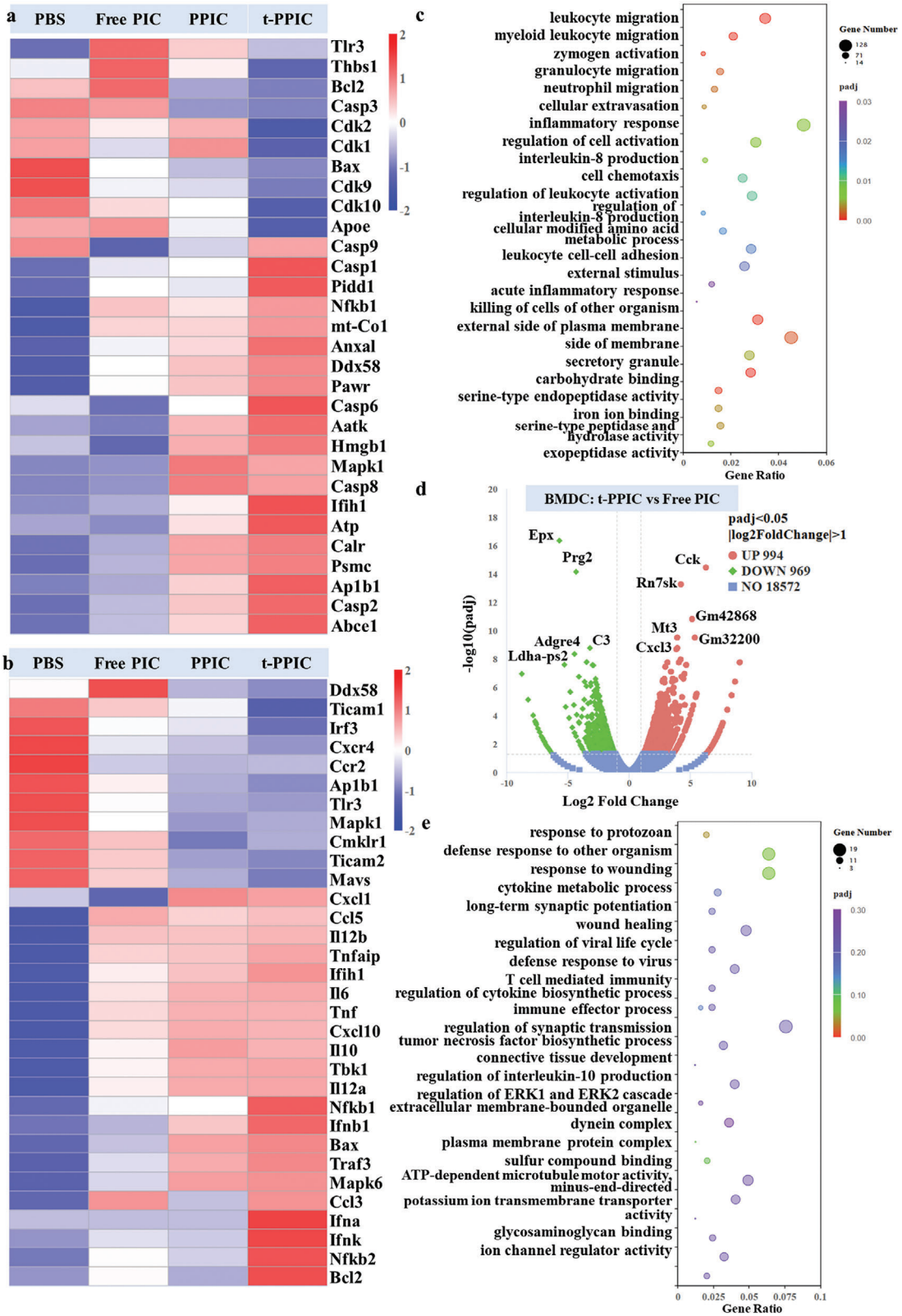

Figure 3. RNA-seq analyses of DCs and LLC cells treated with PIC formulations. Heatmaps of a) LLC cells and b) DCs treated with free PIC and t-PPIC. c) GO analysis of differentially expressed genes (DEGs) in LLC cells. d) Volcano plot and e) GO analysis of DEGs in DCs treated with free PIC or t-PPIC.

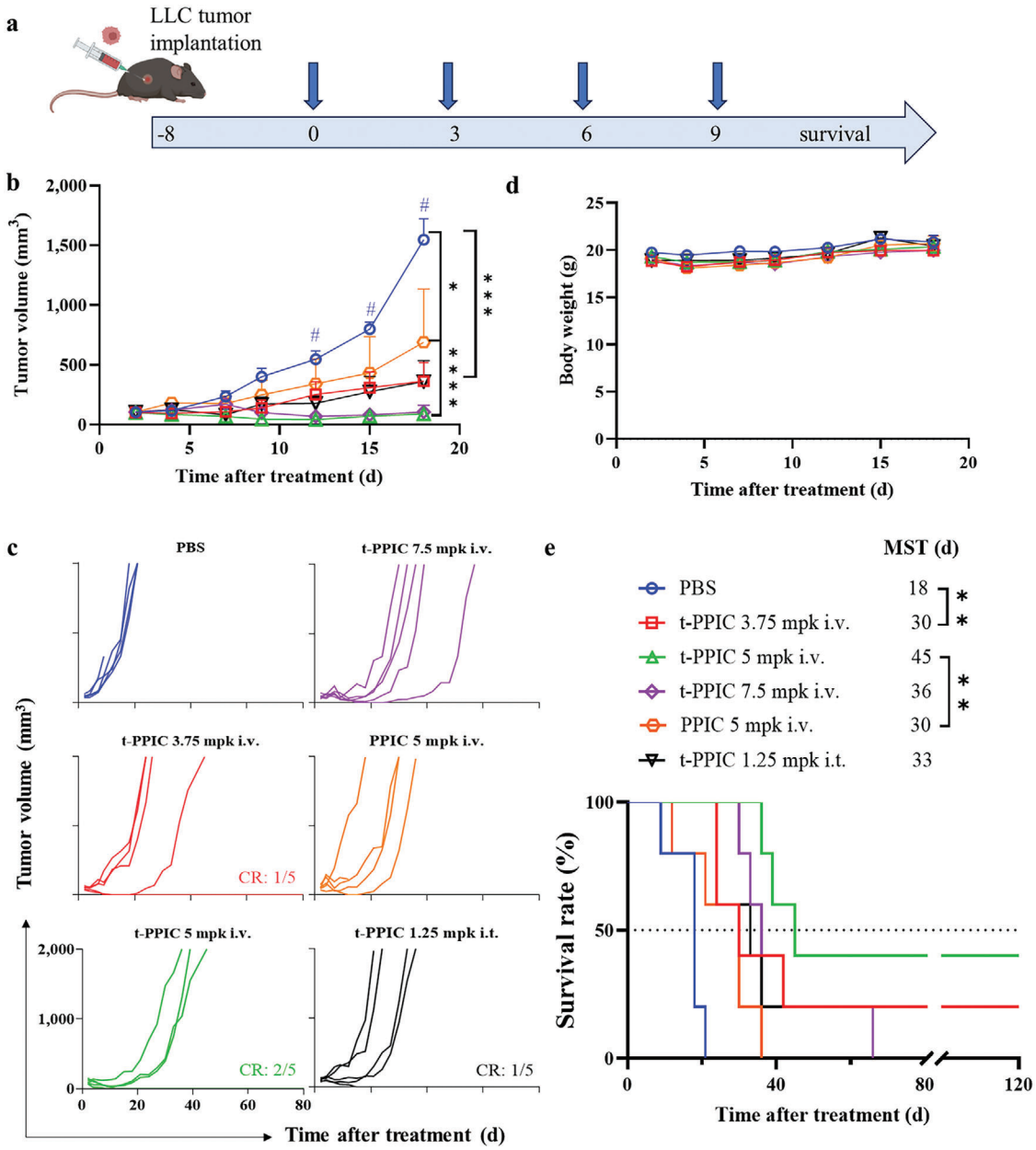

Figure 4. Therapeutic activity of t-PPIC via intravenous (i.v.) or intratumoral (i.t.) injection in a subcutaneous LLC mouse model (n = 5). a) Workflow. b) Average tumor growth curves, c) individual tumor growth curves (CR: cure rate), d) body weights, and e) survival curves of the mice. *$p < 0.05$, **$p < 0.01$, ***$p < 0.001$ and ****$p < 0.0001$.

2.6. Immunological Analyses of the t-PPIC-Treated LLC Model

To elucidate immune microenvironment regulation, we performed immunological analyses of the tumors, spleens, and lymph nodes (LNs) of LLC tumor-bearing mice at 48 h after two intravenous injections of t-PPIC (**Figure 5a**). Figure 5b shows that the tumor volume of the t-PPIC group was the smallest among all the groups, and free PIC treatment resulted in limited tumor suppression, which is consistent with previous reports.[32] In the tumor microenvironment (TME), mDCs and NK cells are the central APCs for an effective immune response. Notably, t-PPIC induced ca. fivefold DC maturation (4.9%, ***p) and threefold NK recruitment (1.2%, *p) compared to those in the PPIC, free PIC, and PBS groups (Figure 5c,d). This was ascribed to better uptake of t-PPIC by APCs, which led to direct stimulation, and better uptake by LLC cells, which resulted in more ICD and APC stimulation. The tumor infiltration of $CD8^+$ T (CTL) and $CD4^+$ T cells increased from the PBS group to the free PIC, PPIC, and t-PPIC groups (Figure 5e,f) due to the recruitment and activation of DCs and NK cells, in line with previous reports.[35] CTLs are the most important effector cells in the adaptive immune response and can directly kill tumor cells. Moreover, t-PPIC and PPIC diminished the immunosuppressive TME, as indicated by decreased levels of Tregs and M2M/M1M (Figure S7a,b, Supporting

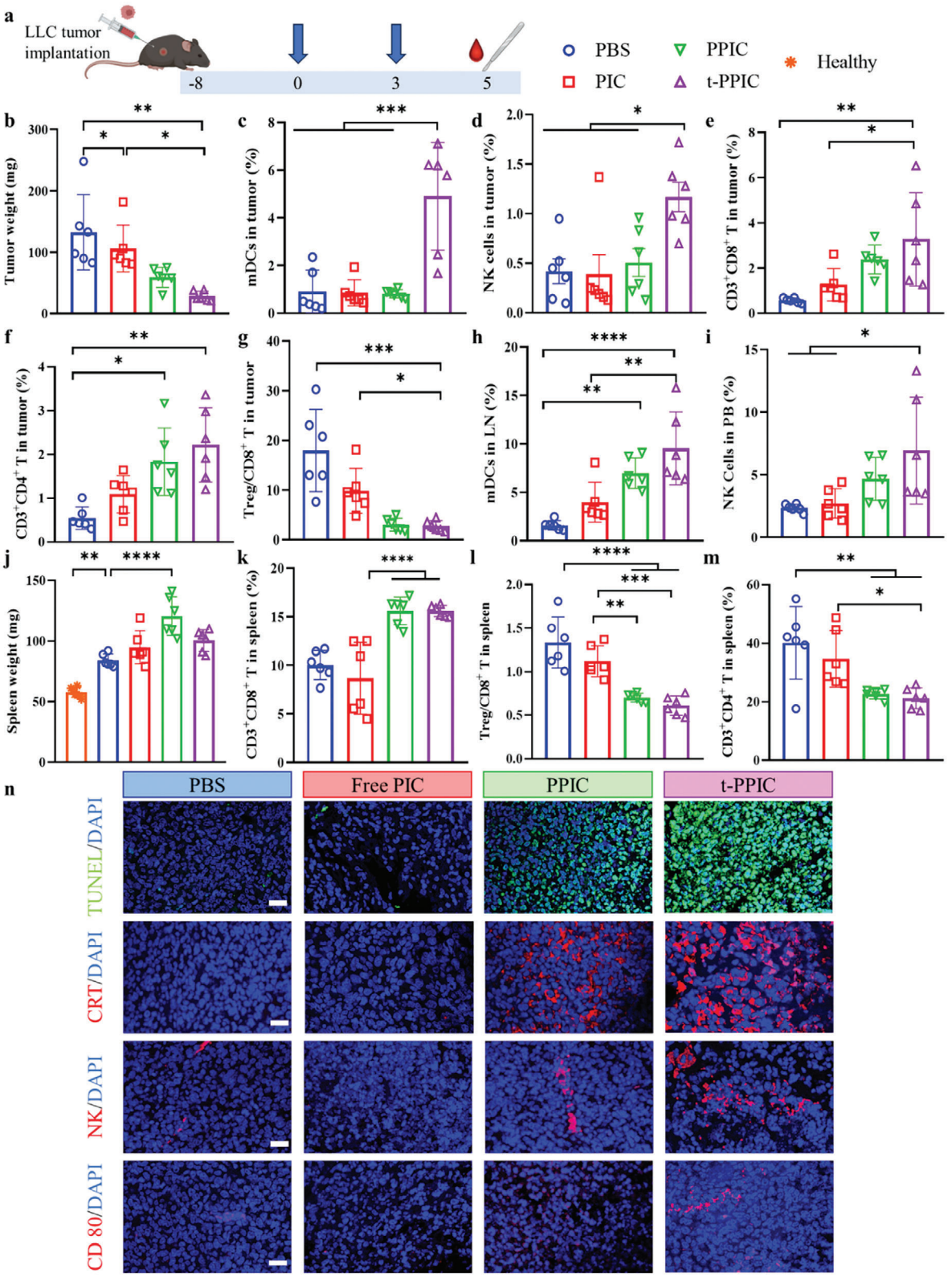

Figure 5. Immunological analysis of t-PPIC-treated LLC mice (n = 6). a) Workflow of immunotherapy using t-PPIC formulations. b) The weights, and percentages of c) mDCs, d) NK cells, e) $CD3^+CD8^+$ T cells, f) $CD3^+CD4^+$ T cells, and g) ratio of Tregs/$CD8^+$ T cells of the tumors in LLC mice. Percentages of h) mDCs in the lymph nodes and i) NK cells in the peripheral blood. j) The average weights, k) $CD3^+CD8^+$ T cells, l) ratio of Treg/$CD8^+$ T cells, and m) $CD3^+CD4^+$ T cells of the spleens of LLC mice. *$p < 0.05$, **$p < 0.01$, ***$p < 0.001$ and ****$p < 0.0001$. n) Tumor slices stained with TUNEL, anti-CRT, anti-NKR, or anti-CD80 antibodies (scale bars: 25 μm).

Information) and a 5- to 6-fold lower ratio of Treg/CD8$^+$ T cells (Figure 5g), confirming that the reshaping of the TME was favorable for immunogenicity. The gating strategies applied in the analysis of immune cells in tumors are illustrated in Figure S8 (Supporting Information). Notably, 60% of the mice were not cured and died within 45 days despite t-PPIC treatment, which may be due to insufficient induction of antigens and/or unsatisfactory inhibition of Treg, M2M, and MSDC by t-PPIC treatment alone, thus warranting further investigation of the combination therapy of t-PPIC with RT and CTLA-4 antibody.

Notably, the t-PPIC group showed significantly more mDCs in the LNs (9.5%) and more NK cells in the peripheral blood (PB, 6.8%) than did the free PIC group (Figure 5h,i), both of which were much greater than those in tumors, verifying the strong systemic immune response of t-PPIC. All LLC mice experienced splenomegaly, possibly because of strong immune stimulation and massive infiltration of immune cells in the spleen (Figure 5j). Compared to those in the free PIC and PBS groups, the number of CD8$^+$ T cells in the PPIC and t-PPIC groups was greater (Figure 5k, ****p), and the levels of immunosuppressive factors, such as Treg/CD8$^+$ T cells (Figure 5l), and the levels of MDSCs and Tregs were similar (Figure S7c,d, Supporting Information). Moreover, total CD8$^+$ and CD4$^+$ T cells accounted for ≈90% of the total CD45$^+$CD3$^+$ T cells in the spleen of the PBS group (Figure S7e, Supporting Information), with only 10% of the total CD8$^+$ T cells but 40% of the total CD4$^+$ T cells in the spleen (Figure 5k,m), which was also reported for other LLC models[36] compared to the percentages in healthy C57BL/6J female mice (CD8$^+$ T cells: 17.9% and CD4$^+$ T cells: 18.8%[37]). The abnormal numbers of CD8$^+$ and CD4$^+$ T cells in the spleen may be associated with high immunosuppression in LLC mice (12% Tregs; Figure S7d, Supporting Information). Remarkably, t-PPIC and PPIC treatment effectively restored CD8$^+$ T and CD4$^+$ T cells to normal levels in healthy spleens and decreased Treg/CD8$^+$ T cells (Figure 5k,m), while free PIC did not reverse these effects.

TUNEL and immunohistological analyses of tumor slices verified the extremely high levels of apoptosis (TUNEL) and ICD (CRT), as well as the clear increase in NK cells and CD80$^+$ mDCs induced by t-PPIC treatment (Figure 5n). Taken together, t-PPIC induced tumor cell apoptosis and generated ICDs that, on the one hand, stimulated DCs and recruited NK cells and, on the other hand, facilitated their endocytosis by APCs in vivo, leading to the colocalization of antigens and adjuvants in APCs and serving as an in situ cancer vaccine.

2.7. Investigation of Combination Therapy of t-PPIC with ICB or RT in LLC Mice

Next, we explored whether t-PPIC could boost ICB therapy and radiation therapy (RT), which present challenges in the clinic.[38] A CTLA-4 antibody (Ab, i.v., 1.0 mpk) or fractionated X-ray (RT, 3 Gy) was combined with t-PPIC (i.v., 5 mpk) to treat LLC mice (**Figure 6a**). Interestingly, the results revealed that the combination of t-PPIC with Ab given one day later (t-PPIC+Ab, combo 1) further reduced the average tumor volume compared with t-PPIC monotherapy, resulting in 60% of the mice cured in the end (Figure 6b,c) without body weight loss (Figure 6d). Since α-CTLA4 monotherapy was reported to be unable to arrest LLC tumor growth,[39] the results confirmed the synergetic effect of t-PPIC and α-CTLA4. Moreover, the combination of RT used 6 h before t-PPIC injection (RT+t-PPIC, combo 2) achieved 80% tumor clearance before day 50, although one tumor relapsed afterward, resulting in 60% tumor-free mice (Figure 6c,e). t-PPIC and the two combo treatments induced widespread and massive tumor cell death, as shown by H&E-stained sections (Figure S9, Supporting Information). In addition, H&E-stained images revealed that the main organs in the PPIC, t-PPIC, and combo groups were not damaged. However, these treatments improved the conditions of the mice in the PBS group, which exhibited interstitial edema and thickening of the alveolar walls of the lung and abnormally increased white pulp of the spleen (Figure S10, Supporting Information). These results underscore the good biosafety of the t-PPIC and combo groups.

Immunological analyses were performed to elucidate the mechanism of enhanced antitumor activity by combination therapies compared with t-PPIC monotherapy (**Figure 7a**). Neither α-CTLA4 nor RT monotherapy influenced tumor inhibition, in agreement with earlier reports,[39] nor did it influence DC activation or NK cell recruitment (Figure 7b–d), but it increased CD8$^+$ T and CD4$^+$ T cells and decreased Treg/CD8$^+$ T cells in tumors compared to those in the PBS group (Figure 7e–g). In general, the two combo treatments further enhanced the efficacy of t-PPIC monotherapy, resulting in enhanced DC activation, NK cell recruitment, and tumor infiltration of CD8$^+$ T cells (Figure 7c,d,f) without additional toxicity. Specifically, combo 1 therapy stimulated mDCs in tumors and LNs with the fewest Treg/CD8$^+$ T cells (Figure 7c,h,g), while combo 2 therapy bolstered significantly increased NK cell recruitment in tumors (****p, Figure 7d) and prevented splenomegaly (Figure 7j). Nevertheless, similar to RT monotherapy, combo 2 increased the immunosuppressive network (Figure S11, Supporting Information); e.g., Treg- and M2M/M1M-mediated radioresistance was reported for RT treatment,[40] which might explain 20% of tumor relapse after 50 d (Figure 6c). Here, compared to RT monotherapy, the combination of t-PPIC (combo 2) could offset the immunosuppressive effect of X-rays by significantly augmenting tumor infiltration of immuno-promoting immune cells, e.g., NK cells, mDCs and CTLs, which directly kill tumor cells, thus greatly improving the cure rate to 60% with no tumor relapse in 120 days. Moreover, the results of IHC (immunohistochemistry) staining of the tumor slices confirmed that tumor infiltration of NK-, CD80- and CD8-positive immune cells was significantly greater in the two combo groups than in the monotherapy groups (Figure 7n), which was in line with the results of flow cytometric analyses.

3. Conclusion

We have demonstrated that integrin-targeted polymersomal poly(I:C) (t-PPIC) can induce self-enhanced and systemic immunotherapy in a murine LLC lung cancer model. This t-PPIC is ≈52 nm in size and shows greatly improved uptake both by tumor cells and APCs that overexpress $\alpha_v\beta_3$ and $\alpha_v\beta_5$ integrins. Additionally, t-PPIC markedly enhanced ICD and DC maturation, acting as a powerful in situ antitumor vaccine. Remarkably, i.v. administration of t-PPIC at a dose of 5 mpk significantly suppressed tumor growth and enhanced survival rate, with 40% of the mice becoming tumor-free. Immunological analyses con-

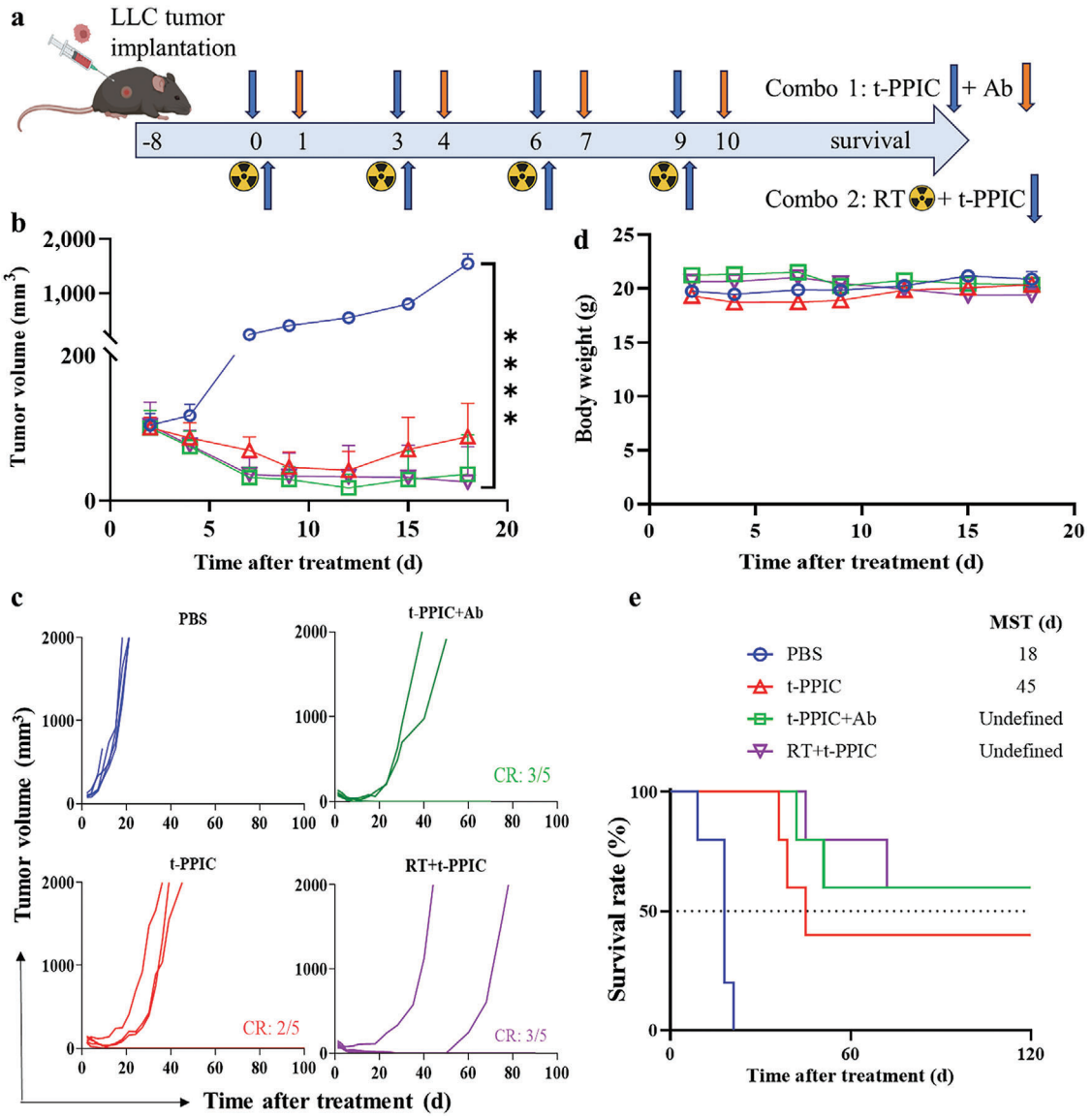

Figure 6. Therapeutic activity of t-PPIC (i.v., 5 mpk) in combination with α-CTLA-4 (Ab, i.v., 1.0 mpk) or fractionated X-ray (RT, 3 Gy) in LLC mice (n = 5). a) Workflow. b) Average tumor growth curves, c) individual tumor growth curves (CR: cure rate), d) body weights, and e) survival curves of the mice. ****$p < 0.0001$.

firmed extensive ICD within the tumor tissue, greatly enhanced maturation of DCs, and the recruitment of NK cells and $CD8^+$ T cells. Furthermore, combining t-PPIC with anti-CTLA4 therapy or radiotherapy further enhanced its antitumor effect, resulting in 60% complete regression. This "one-component" integrin-targeted nanopoly(I:C) represents an exciting new strategy for safe, potent, and durable immunotherapy against solid tumors.

4. Experimental Section

Fabrication and Characterization of the Nano-TLR3 Agonist (t-PPIC): Polymersomal poly(I:C) (PPIC) was facilely obtained by adding 100 µL of PEG-P(TMC-DTC)-sp solution in DMF (50 mg mL^{-1}) to 900 µL of HEPES buffer (pH 6.8, 5 mM) containing various PIC (2.5 to 10 mg mL^{-1}) at a theoretical loading content ranging from 5 wt.% – 20 wt.%. To prepare integrin-targeting nanopoly(I:C) (t-PPIC), the procedure was the same, except that cRGD-PEG-P(TMC-DTC) was premixed with 20 wt.% PEG-P(TMC-DTC)-sp. To prepare Cy5-labeled t-PPIC for the endocytosis study, the procedure was the same as that described above, except that 1 wt.% Cy5-labeled PEG-P(TMC-DTC) was premixed. The size, size distribution, morphology, and drug loading of PPIC and t-PPIC were measured, and the stability of the polymersomes (1 mg mL^{-1}) at 4 C, in the presence of 10% FBS or GSH (10 mM) was investigated using DLS and gel electrophoresis.

Apoptosis, Colony Formation and ICD Induction of LLC Cells Induced by t-PPIC: LLC cells seeded on a 6-well plate (1×10^5/well) overnight were treated with PPIC or t-PPIC (PIC conc.: 1, 5, 10, 50 µg mL^{-1}). After 24 h, the cells were washed, counted, and reinoculated in a new 6-well plate at 500/well to form clones. The medium was changed every 3 days. After 15 days, the cells and clones were fixed and stained with crystal violet for 10 min. After washing, the cells were dried and photographed with a camera.

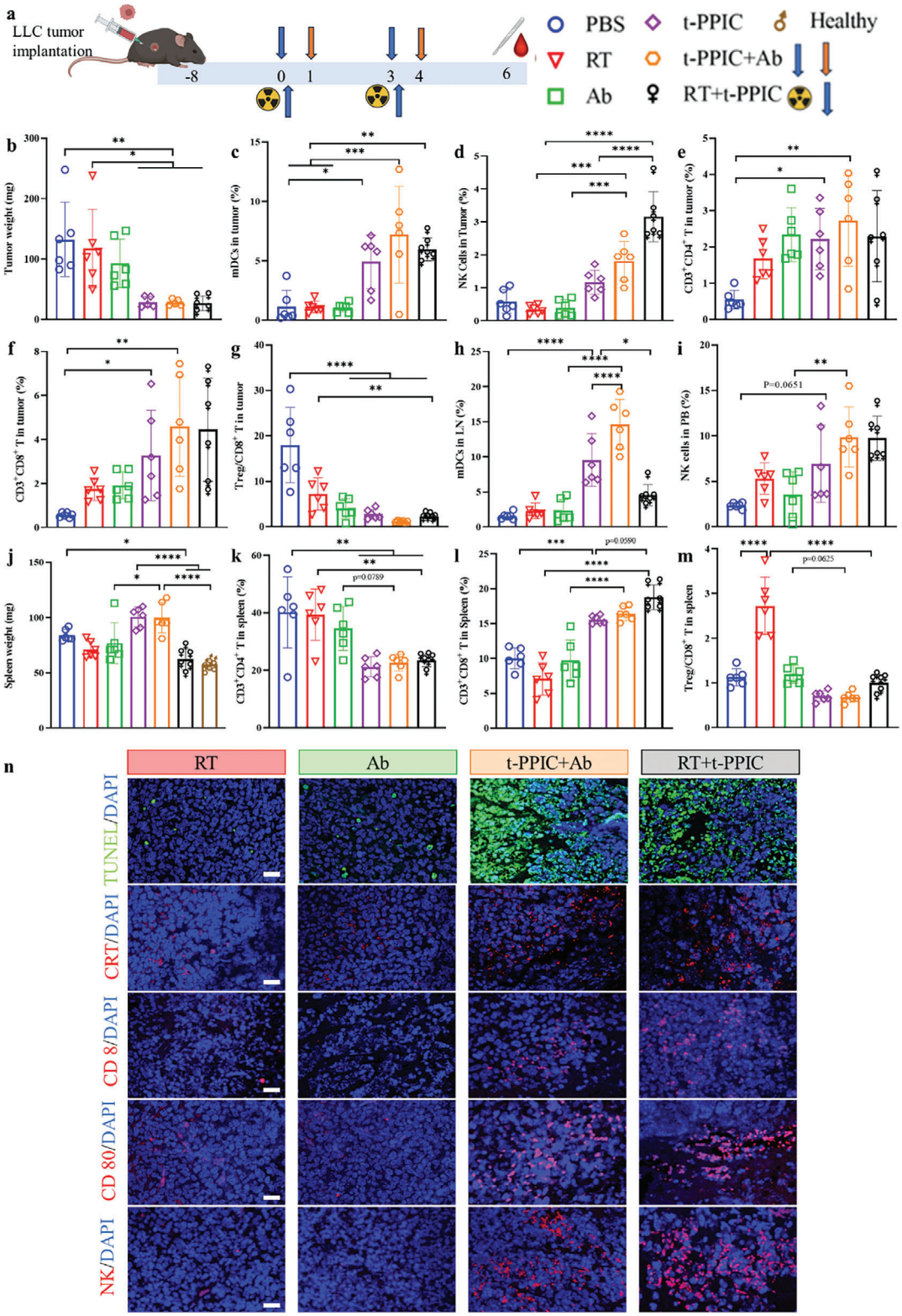

Figure 7. Immunological analyses of LLC mice treated with t-PPIC (i.v., 5 mpk) in combination with an α-CTLA-4 antibody (Ab, i.v., 1.0 mpk) or fractionated X-ray (RT, 3 Gy) (n = 6). a) Workflow. b) Body weights, the contents of c) mDCs, d) NK cells, e) $CD3^+CD4^+$ T cells, f) $CD3^+CD8^+$ T cells, and g) the ratio of Tregs/$CD8^+$ T cells in the tumors of LLC mice. The percentage of h) mDCs in lymph nodes and i) NK cells in peripheral blood. j) The average weights, percentages of k) $CD3^+CD4^+$ T cells, l) $CD3^+CD8^+$ T cells, and m) percentages of Treg/$CD8^+$ T cells in the spleens of LLC mice. $^*p < 0.05$, $^{**}p < 0.01$, $^{***}p < 0.001$ and $^{****}p < 0.0001$. n) Tumor slices stained with TUNEL, anti-CRT, anti-CD8, anti-CD80, or anti-NKR antibodies (scale bars: 25 μm).

To study the apoptosis of LLC cells, the cells seeded in 12-well plates (5×10^4/well) overnight were incubated with PBS, free PIC, PPIC, or t-PPIC (PIC conc.: 10 μg mL^{-1}) for 48 h. The cells were digested with Accutase, centrifuged (500 rpm, 8 min) and stained with Annexin V-APC/7-AAD according to the protocol followed by flow cytometry (FC) measurement.

To study ICD induction, LLC cells seeded in a 6-well plate (1×10^5/well) overnight were incubated with PBS, free PIC, PPIC, or t-PPIC (PIC conc.: 10 μg mL^{-1}, n = 3). After 24 h, the culture medium was taken to measure the ATP concentration using an ATP assay kit. The cells were digested with trypsin, washed (PBS 2×), and incubated with blocking antibody at 4 C for 20 min before 1 h of incubation with anti-CRT antibody at room temperature. The cells were washed with PBS 3×, incubated with Alexa Fluor 647 for 30 min, and subjected to FC measurement. 4T1 cells and GL261 cells were seeded in 6-well plates (3×10^5/well) overnight, treated and measured using the same procedure as above.

RNA-Seq Analyses of LLC Cells and BMDCs Treated with t-PPIC: LLC cells (7×10^5/well) and BMDCs (2×10^6/well) cultured in 6-well plates as described above were incubated with t-PPIC, PPIC, or free PIC (PIC conc.: 50 μg mL^{-1}). After 24 h, the cells were collected and washed with PBS, 1 mL of TRIzol was added, and the cells were stored at −80 C before analysis. RNA-seq library construction and testing were performed at Beijing Novogene. Heatmaps were generated, and volcano and GO differential analyses were performed using the Novomagic platform.

Activation and Antigen Presentation of APCs: To study the activation of BMDCs by t-PPIC, BMDCs in a 12-well plate (1×10^6/well) were incubated with PBS, PIC, PPIC or t-PPIC for 24 h (PIC conc.: 10 μg mL^{-1}, n = 3). The cells were collected and incubated with FITC-conjugated anti-αCD11c, APC-conjugated anti-CD80 and PE-conjugated anti-αCD86 antibodies at 4 C for 30 min. After washing with PBS, the cells were resuspended in PBS, and FC measurements were performed.

To study the activation of BMDCs by coculturing t-PPIC and LLC cells, 100 μL of t-PPIC (PIC conc.: 10 μg mL^{-1}) and 1 mL of BMDCs (1×10^6/well, RPMI-1640 medium) were added to LLC cells seeded in a 12-well plate (1×10^5/well, 900 μL of DMEM) overnight (n = 3). After 24 h, all cells were centrifuged and stained with Per/Cy5.5-αCD45 to distinguish immune cells from tumor cells and then stained with antibodies and quantified by FC as described above.

To study the antigen presentation of BMDCs treated with t-PPIC, BMDCs seeded in a 12-well plate (1×10^6/well) were treated with the model antigen OVA (1 μg mL^{-1}) and then cocultured with PBS, PIC, PPIC, or t-PPIC (PIC conc.: 10 μg mL^{-1}, n = 3). After 24 h, the cells were centrifuged, washed, and labeled with FITC-αCD11c, APC-αCD80, PE-αCD86, and Per/Cy5.5-I-A/I-E (MHC-II) antibodies at 4 C for 30 min. The cells were subsequently washed and resuspended in PBS for FC measurement.

Therapeutic Activity of t-PPIC in LLC Tumor-Bearing Mice: All animal procedures were performed by the Guidelines for Care and Use of Laboratory Animals of Soochow University (P. R. China) and approved by the Animal Ethics Committee of Soochow University. The approval number for the animal experiments was SYXK (Jiangsu) 2021-0065. The LLC tumor-bearing mouse model was established in the same way as above. At a tumor volume of 80–100 mm^3 (day 0), the mice were randomly grouped according to the PIC formulation, dose (in mg kg^{-1}, mpk) and administration method (n = 5): PBS, t-PPIC (3.75 mpk, i.v.), t-PPIC (5 mpk, i.v.), t-PPIC (7.5 mpk, i.v.), PPIC (5 mpk, i.v.), and t-PPIC (1.25 mpk, i.t.). The drugs were given on days 0, 3, 6, and 9. The tumor volume and body weight of the mice were monitored every 3 days. The survival rates were recorded at mouse death or when the tumor volume exceeded 2000 mm^3.

To investigate the enhancing effect of t-PPIC on ICB or RT in LLC mice, t-PPIC combined with α-CTLA4 (Ab) or 3 Gy X-ray (RT) was used. The mice were divided into four groups (n = 5): PBS, t-PPIC, t-PPIC+Ab (combo 1), and RT+ t-PPIC (combo 2). t-PPIC was administered at 5 mpk (i.v.) on days 0, 3, 6, and 9. For combo 1, α-CTLA4 was i.v. injected (Ab: 1 mpk) at 24 h after each t-PPIC on days 1, 4, 7, and 10. For combo 2, X-ray irradiation (RT: 3 Gy) was conducted 6 h before each t-PPIC. The tumor volume, body weight, and survival rates were recorded.

Immunological Analyses of LLC Mice after t-PPIC Therapy or Combination Therapy: LLC mice with a tumor volume of 100 mm^3 were randomly divided into 4 groups (n = 6): PBS, free PIC, PPIC or t-PPIC (PIC: 5 mpk, i.v.), and formulations were injected on days 0 and 3. On day 5, five mice from each group were sacrificed, and the blood and inguinal lymph nodes (LNs) were collected to determine the percentages of NK cells and mDCs ($CD45^+CD11c^+CD80^+CD86^+$). The spleens and tumors were weighed and ground into single-cell suspensions. The numbers of $CD8^+$ T ($CD45^+CD3^+CD8^+$), $CD4^+$ T ($CD45^+CD3^+CD4^+$), and Treg ($CD45^+CD3^+CD4^+FoxP3^+$) cells and MDSCs ($CD11b^+Gr\text{-}1^+$) in the spleen were analyzed. The proportions of mDCs, NK cells, M2Ms ($CD11b^+F4/80^+CD206^+$), M1Ms ($CD11b^+F4/80^+CD206^-$), and T cells (Treg, $CD4^+$T and $CD8^+$T cells) in the tumors were measured using FC and analyzed using FlowJo_V10 software. One mouse from each group was sacrificed, and the main organs and tumors were excised and stained with hematoxylin and eosin (H&E) for light microscopic observation. The tumor slices were also subjected to TUNEL and IHC (CRT, CD8, CD80 and NK primary antibodies and Alexa Fluor 647 secondary antibody) staining and observed via Confocal laser scanning microscope (CLSM).

To study the effect of the combination treatment, LLC mice were randomly divided into 6 groups (n = 6): PBS, RT, Ab, t-PPIC, t-PPIC+Ab, and RT+t-PPIC (t-PPIC: 5 mpk i.v., Ab:1 mpk i.v. RT: 3 Gy). t-PPIC (5 mpk i.v.) was given on days 0 and 3. α-CTLA4 (Ab: 1 mpk i.v.) was injected 24 h after each t-PPIC injection on days 1 and 4, and X-ray (3 Gy) was applied 6 h before each t-PPIC injection. The tumors, LNs, and spleens were treated and measured as described above.

Statistical Analysis: Data are presented as the mean ± SD unless otherwise stated. Differences among groups were evaluated using one-way ANOVA with Tukey's multiple comparison test, and survival curves were estimated using the Kaplan–Meier method with a log-rank comparison test in GraphPad Prism 8 software. *$p < 0.05$ indicates significance, and **$p < 0.01$, ***$p < 0.001$ and ****$p < 0.0001$ indicate high significance.

Supporting Information

Supporting Information is available from the Wiley Online Library or from the author.

Acknowledgements

This work is supported by research grants from the National Natural Science Foundation of China (NSFC 52033006, 52233007) and the National Key Research and Development Program of China (2022YFA1206000).

Conflict of Interest

The authors declare no conflict of interest.

Data Availability Statement

The data that support the findings of this study are available in the supplementary material of this article.

Keywords

active targeting, immunotherapy, lung cancer, polymersomes, toll-like receptor 3

Received: February 28, 2024
Revised: June 18, 2024
Published online: June 27, 2024

[1] a) T. K. Kim, E. N. Vandsemb, R. S. Herbst, L. Chen, *Nat. Rev. Drug Discov.* **2022**, *21*, 529; b) Z. Hu, P. A. Ott, C. J. Wu, *Nat. Rev. Immunol.* **2018**, *18*, 168.

[2] F. Zhou, M. Qiao, C. Zhou, *Cell Mol. Immunol.* **2021**, *18*, 279.
[3] Y. Zhu, X. Yu, S. D. Thamphiwatana, Y. Zheng, Z. Pang, *Acta Pharm. Sin. B.* **2020**, *10*, 2054.
[4] J. De Waele, T. Verhezen, S. van der Heijden, Z. N. Berneman, M. Peeters, F. Lardon, A. Wouters, E. Smits, *J. Exp. Clin. Cancer Res.* **2021**, *40*, 213.
[5] A. I. Chin, A. K. Miyahira, A. Covarrubias, J. Teague, B. Guo, P. W. Dempsey, G. Cheng, *Cancer Res.* **2010**, *70*, 2595.
[6] a) F. Bianchi, S. Pretto, E. Tagliabue, A. Balsari, L. Sfondrini, *Cancer Biol. Ther.* **2017**, *18*, 747; b) Z. Urban-Wojciuk, M. M. Khan, B. L. Oyler, R. Fahraeus, N. Marek-Trzonkowska, A. Nita-Lazar, T. R. Hupp, D. R. Goodlett, *Front. Immunol.* **2019**, *10*, 02388.
[7] D. Wu, Z. Wang, J. Zhang, A. G. Robinson, B. Lyu, Z. Chen, C. Wang, B. Wei, X. Xia, Q. Zhang, X. Zhou, *Cell Death Dis.* **2022**, *13*, 731.
[8] J. Fucikova, O. Kepp, L. Kasikova, G. Petroni, T. Yamazaki, P. Liu, L. Zhao, R. Spisek, G. Kroemer, L. Galluzzi, *Cell Death Dis.* **2020**, *11*, 1013.
[9] C. S. Lu, C. W. Lin, Y. H. Chang, H. Y. Chen, W. C. Chung, W. Y. Lai, C. C. Ho, T. H. Wang, C. Y. Chen, C. L. Yeh, S. Wu, S. P. Wang, P. C. Yang, *J. Immunother. Cancer* **2020**, *8*, e001392.
[10] a) H. Zhou, H. He, R. Liang, H. Pan, Z. Chen, G. Deng, S. Zhang, Y. Ma, L. Liu, L. Cai, *Biomaterials* **2021**, *269*, 120670; b) A. Lamoot, S. Jangra, G. Laghlali, P. Warang, G. Singh, L. A. Chang, S. C. Park, G. Singh, K. De Swarte, Z. Zhong, B. Louage, E. De Lombaerde, T. Ye, Y. Chen, S. Cuadrado-Castano, S. Lienenklaus, N. N. Sanders, B. N. Lambrecht, A. Garcia-Sastre, M. Schotsaert, B. G. De Geest, *Small* **2024**, *20*, 2306892; c) E. C. Gale, G. A. Roth, A. A. A. Smith, M. Alcántara-Hernández, J. Idoyaga, E. A. Appel, *Adv. Ther.* **2019**, *3*, 1900174; d) P. P. Zhang, Y. C. Chiu, L. H. Tostanoski, C. M. Jewell, *ACS Nano* **2015**, *9*, 6465; e) L. Yang, X. Wang, Y. Zhao, Y. Li, X. Wang, J. Deng, Z. Qi, *Chem. Eng. J.* **2023**, *473*, 145205.
[11] L. Ma, L. Diao, Z. Peng, Y. Jia, H. Xie, B. Li, J. Ma, M. Zhang, L. Cheng, D. Ding, X. Zhang, H. Chen, F. Mo, H. Jiang, G. Xu, F. Meng, Z. Zhong, M. Liu, *Adv. Mater.* **2021**, *33*, 2104849.
[12] N. Benne, J. van Duijn, J. Kuiper, W. Jiskoot, B. Slutter, *J. Controlled Release* **2016**, *234*, 124.
[13] A. Schudel, D. M. Francis, S. N. Thomas, *Nat. Rev. Mater.* **2019**, *4*, 415.
[14] M. Beygi, F. Oroojalian, S. S. Hosseini, A. Mokhtarzadeh, P. Kesharwani, A. Sahebkar, *Prog. Mater. Sci.* **2023**, *140*, 101209.
[15] a) H. Zheng, B. Guo, X. Qiu, Y. Xia, Y. Qu, L. Cheng, F. Meng, Z. Zhong, *Bioact Mater* **2022**, *16*, 1; b) D. Li, J. Li, S. Wang, W. Teng, Q. Wang, *Int. J. Nanomed.* **2022**, *17*, 5679; c) N. Yu, Y. Zhang, J. Li, W. Gu, S. Yue, B. Li, F. Meng, H. Sun, R. Haag, J. Yuan, Z. Zhong, *Adv. Mater.* **2021**, *33*, 2007787; d) G. Cui, Y. Sun, L. Qu, C. Shen, Y. Sun, F. Meng, Y. Zheng, Z. Zhong, *Adv. Healthcare Mater.* **2024**, 2303690; e) S. Wang, G. Yu, W. Yang, Z. Wang, O. Jacobson, R. Tian, H. Deng, L. Lin, X. Chen, *Adv. Sci.* **2021**, *8*, 2002927; f) Y. Zou, M. Zheng, W. Yang, F. Meng, K. Miyata, H. J. Kim, K. Kataoka, Z. Zhong, *Adv. Mater.* **2017**, *29*, 1703285.
[16] a) H. Javid, M. A. Oryani, N. Rezagholinejad, A. Esparham, M. Tajaldini, M. Karimi-Shahri, *Cancer Med.* **2024**, *13*, e6800; b) W. Zhuo, W. Wang, W. Zhou, Z. Duan, S. He, X. Zhang, L. Yi, R. Zhang, A. Guo, X. Gou, J. Chen, N. Huang, X. Sun, Z. Qian, X. Wang, X. Gao, *Small* **2024**, e2400630; c) B. Li, H. Niu, X. Zhao, X. Huang, Y. Ding, K. Dang, T. Yang, Y. Chen, J. Ma, X. Liu, K. Zhang, H. Xie, P. Ding, *Asian J. Pharm. Sci.* **2024**, *19*, 100891.
[17] K. S. de Valk, M. M. Deken, H. J. M. Handgraaf, S. S. Bhairosingh, O. D. Bijlstra, M. J. van Esdonk, A. G. T. Terwisscha van Scheltinga, A. Valentijn, T. L. March, J. Vuijk, K. Peeters, F. A. Holman, D. E. Hilling, J. S. D. Mieog, J. V. Frangioni, J. Burggraaf, A. L. Vahrmeijer, *Clin. Cancer Res.* **2020**, *26*, 3990.
[18] Z. Wang, S. Zhao, J. Shi, F. Meng, J. Yuan, Z. Zhong, *Acta Biomater.* **2022**, *138*, 443.
[19] M. Caskey, F. Lefebvre, A. Filali-Mouhim, M. J. Cameron, J. P. Goulet, E. K. Haddad, G. Breton, C. Trumpfheller, S. Pollak, I. Shimeliovich, A. Duque-Alarcon, L. Pan, A. Nelkenbaum, A. M. Salazar, S. J. Schlesinger, R. M. Steinman, R. P. Sekaly, *J. Exp. Med.* **2011**, *208*, 2357.
[20] J. Wei, D. Wu, Y. Shao, B. Guo, J. Jiang, J. Chen, J. Zhang, F. Meng, Z. Zhong, *J. Controlled Release.* **2022**, *347*, 68.
[21] a) Y. L. Chen, M. C. Chang, Y. C. Chiang, H. W. Lin, N. Y. Sun, C. A. Chen, W. Z. Sun, W. F. Cheng, *Cancer Lett.* **2018**, *425*, 152; b) S. Yoshida, H. Shime, Y. Takeda, J. M. Nam, K. Takashima, M. Matsumoto, H. Shirato, M. Kasahara, T. Seya, *Cancer Sci.* **2018**, *109*, 956.
[22] H. Harjunpaa, M. Llort Asens, C. Guenther, S. C. Fagerholm, *Front. Immunol.* **2019**, *10*, 01078.
[23] S. E. Ackerman, C. I. Pearson, J. D. Gregorio, J. C. Gonzalez, J. A. Kenkel, F. J. Hartmann, A. Luo, P. Y. Ho, H. LeBlanc, L. K. Blum, S. C. Kimmey, A. Luo, M. L. Nguyen, J. C. Paik, L. Y. Sheu, B. Ackerman, A. Lee, H. Li, J. Melrose, R. P. Laura, V. C. Ramani, K. A. Henning, D. Y. Jackson, B. S. Safina, G. Yonehiro, B. H. Devens, Y. Carmi, S. J. Chapin, S. C. Bendall, M. Kowanetz, et al., *Nat. Cancer* **2021**, *2*, 18.
[24] L. Xu, W. Zhang, H. B. Park, M. Kwak, J. Oh, P. C. W. Lee, J. O. Jin, *J. Immunother. Cancer* **2019**, *7*, 220.
[25] S. C. Chang, B. X. Zhang, E. C. Su, W. C. Wu, T. H. Hsieh, A. M. Salazar, Y. K. Lin, J. L. Ding, *Int. J. Mol. Sci.* **2021**, *22*, 1626.
[26] G. P. Mishra, A. Jha, A. Ahad, K. Sen, A. Sen, S. Podder, S. Prusty, V. K. Biswas, B. Gupta, S. K. Raghav, *Cell. Mol. Life Sci.* **2022**, *79*, 429.
[27] A. Nam, S. Jain, C. Wu, A. Campos, R. M. Shepard, Z. Yu, J. P. Reddy, T. Von Schalscha, S. M. Weis, M. Onaitis, H. I. Wettersten, D. A. Cheresh, *Cancer Res.* **2024**, *84*, 1630.
[28] F. Bianchi, S. Alexiadis, C. Camisaschi, M. Truini, G. Centonze, M. Milione, A. Balsari, E. Tagliabue, L. Sfondrini, *Int. J. Mol. Sci.* **2020**, *21*, 1440.
[29] Y. Xia, J. Wei, S. Zhao, B. Guo, F. Meng, B. Klumperman, Z. Zhong, *J. Controlled Release* **2021**, *336*, 262.
[30] Y. Li, X. Jiang, T. Luo, J. Xia, M. J. Lee, R. R. Weichselbaum, W. Lin, *Biomaterials* **2022**, *290*, 121831.
[31] W. Xuan, F. Khan, C. D. James, A. B. Heimberger, M. S. Lesniak, P. Chen, *Trends Cell Biol.* **2021**, *31*, 940.
[32] a) Y. Tong, L. Zhou, L. Yang, P. Guo, Y. Cao, F. X. Qin, J. Liu, *eBioMedicine* **2019**, *39*, 132; b) E. Muller, M. Speth, P. F. Christopoulos, A. Lunde, A. Avdagic, I. Oynebraten, A. Corthay, *Front. Immunol.* **2018**, *9*, 02520.
[33] X. Qiu, Y. Qu, B. Guo, H. Zheng, F. Meng, Z. Zhong, *J. Controlled Release* **2022**, *341*, 498.
[34] F. Baharom, R. A. Ramirez-Valdez, A. Khalilnezhad, S. Khalilnezhad, M. Dillon, D. Hermans, S. Fussell, K. K. S. Tobin, C. A. Dutertre, G. M. Lynn, S. Muller, F. Ginhoux, A. S. Ishizuka, R. A. Seder, *Cell* **2022**, *185*, 4317.
[35] H. Sultan, J. Wu, V. I. Fesenkova, A. E. Fan, D. Addis, A. M. Salazar, E. Celis, *J. Immunother. Cancer* **2020**, *8*, e001224.
[36] Y. S. Tang, W. F. Fan, G. H. Chen, M. Zhang, X. P. Tang, H. R. Wang, P. F. Zhao, Q. Xu, Z. B. Wu, X. X. Lin, Y. Z. Huang, *Nano Today* **2021**, *40*, 101244.
[37] J. A. Hensel, V. Khattar, R. Ashton, S. Ponnazhagan, *Lab. Invest.* **2019**, *99*, 93.
[38] K. B. Pointer, S. P. Pitroda, R. R. Weichselbaum, *Trends Cancer* **2022**, *8*, 9.
[39] R. Thakkar, D. Upreti, S. Ishiguro, M. Tamura, J. Comer, *RSC Med. Chem.* **2023**, *14*, 658.
[40] M. De Martino, C. Daviaud, C. Vanpouille-Box, *Semin. Immunol.* **2021**, *52*, 101474.